

**Instability of pedestrian flow and phase structure in a two-dimensional optimal velocity model**

Akihiro Nakayama\*

*Gifu Keizai University, Ohgaki 503-8550, Japan*Katsuya Hasebe<sup>†</sup>*Faculty of Business Administration, Aichi University, Miyoshi, Aichi 470-0296, Japan*Yūki Sugiyama<sup>‡</sup>*Department of Complex Systems Science, Graduate School of Information Science, Nagoya University, Nagoya, 464-8601, Japan*

(Received 22 October 2004; published 18 March 2005)

A two-dimensional optimal velocity model was proposed for the study of pedestrian and granular flow. We investigate the stability of homogeneous flow in the linear approximation and show the phase diagram of the model. We also investigate the property of the model by numerical simulation in the cases of unidirectional and counter flow. From these results, we present a unified understanding of the behavior of pedestrians and other related systems.

DOI: 10.1103/PhysRevE.71.036121

PACS number(s): 05.70.Fh, 45.70.Vn, 07.05.Tp, 05.90.+m

**I. INTRODUCTION**

In the past decade, traffic and some related systems are investigated from the physical viewpoint of many-particle systems [1–6]. Pedestrian flow is one of such systems and presents interesting phenomena such as lane formation or blocking [7,8]. The behavior of pedestrians has been investigated not only in physics but also in engineering, and various models are proposed to reproduce the phenomena [9–16]. Several models, for example, cellular automata models, have already applied to the realistic problems such as the evacuation from a building or a ship [17,18]. However, these models are tuned to reproduce the behavior of each phenomenon, and the general study of pedestrian flow itself has not been done. Dynamical models for pedestrian flow are useful for such studies, especially for analytical studies, because the motion of pedestrians is described by the dynamical equation of motion. For the general study of pedestrian flow, it is necessary to construct a simple model which can be investigated analytically.

It is well known that there is a similarity among pedestrian flow, traffic flow and granular flow through a pipe. A jam or a similar phenomenon is commonly observed independent of the dimensionality; one-dimensional traffic flow, two-dimensional pedestrian flow and three-dimensional granular flow. Generally, a higher-dimensional system reduces to a lower one in a certain limit. When they have a common property, we expect that the property can be explained by the same mechanism. As a candidate for the model which can explain those phenomena in a unified framework, we adopt the optimal velocity (OV) model [19–21] in the following reasons. The property of one-dimensional traffic flow is well understood by the OV model

and the traffic congestion is interpreted as a phase transition. A density wave similar to traffic congestion is observed in granular flow in liquid through a vertical pipe. In this case, the system can be reduced to quasi-one-dimensional one, which is expressed by a similar equation to the OV model [22,23]. Moreover we can observe a density wave in a special case of pedestrian flow such as a march of children, where the system can be considered as one-dimensional flow. Therefore we can expect that the behavior of pedestrians can be explained in the framework of the OV model or its two-dimensional extension.

We have proposed a two-dimensional OV model, which is a natural extension of the original OV model [24–27]. The OV model for traffic flow is constructed in a simple concept: A driver maintains his optimal velocity depending on the distance to other vehicles. We can easily extend the model to higher-dimensional systems along the same concept. In this model, pedestrians are treated as identical particles moving in the two-dimensional space, and each particle decides its optimal velocity depending on distances to other particles. The model reduces to the original OV model in a special case where particles form a line. In this paper, we show that the model gives a unified understanding of the phenomena in pedestrian flow and in one-dimensional traffic flow. We investigate the linear stability of the homogeneous flow solution. It is shown that the homogeneous flow is unstable if the density exceeds a certain critical value. In this case, the homogeneous distribution of particles is gradually broken, and a density wave emerges spontaneously. Some typical stationary patterns are finally formed depending on the values of parameters. This is the same phenomena as traffic congestion, and can be interpreted as a phase transition from homogeneous flow to congested flow. We also show the existence of a phase which does not exist in a one-dimensional system. Typical profile of flow in each phase can be obtained by use of numerical simulations.

In Sec. II we present the two-dimensional OV model after the brief review of the one-dimensional OV model. We carry out the linear analysis of the homogeneous flow and find the

\*Email address: g44153g@cc.nagoya-u.ac.jp

<sup>†</sup>Email address: hasebe@vega.aichi-u.ac.jp<sup>‡</sup>Email address: genbey@eken.phys.nagoya-u.ac.jp

stability conditions in Sec. III. We also show the phase diagram in this section. In Sec. IV, we show some typical features of the phases by use of numerical simulations. Section V is devoted to summary and discussion.

## II. TWO-DIMENSIONAL OV MODEL

First we briefly review the one-dimensional OV model [19]. The basic concept of the model is that each driver controls the acceleration in order to reduce the difference between the optimal velocity and his real velocity. The model is expressed by the equation of motion

$$\frac{d^2}{dt^2}x_n(t) = a \left[ V(\Delta x_n(t)) - \frac{d}{dt}x_n(t) \right], \quad (1)$$

where  $x_n$  and  $\Delta x_n$  are the position and the headway of the  $n$ th vehicle.  $a$  is ‘‘sensitivity,’’ which represents the strength of reaction of each driver.  $V(\Delta x)$  is ‘‘OV function,’’ which indicates an optimal velocity depending on his headway. We adopt a following form of OV function:  $V(\Delta x) = \alpha[\tanh\beta(\Delta x - b) + c]$ .

This model has a trivial homogeneous flow solution

$$x_n = hn + V(h)t + \text{const}, \quad (2)$$

where all vehicles run with the same velocity  $V(h)$  and the same headway  $h$ . We can find the stability condition of the solution by the linear analysis.

Let  $y_n$  be a small fluctuation on the above solution. The stability condition for the mode solution  $y_n(t) = \exp[in\theta - i\omega(\theta)t]$  is

$$a > V'(h)(1 + \cos \theta). \quad (3)$$

When the condition is not satisfied, the homogeneous flow is unstable for the mode  $\theta$ . If unstable modes exist, the flow transits to a congested flow with jam clusters.

In order to apply the OV model to the phenomena in pedestrian flow, we construct a two-dimensional OV model [24]. This model is a natural extension of the original one-dimensional OV model. Hereafter we call pedestrians as ‘‘particles’’ for convenience.

The equation of motion for a particle with the index  $j$  is given by

$$\frac{d^2}{dt^2}\mathbf{x}_j(t) = a \left[ \left\{ \mathbf{V}_0 + \sum_k \mathbf{F}(\mathbf{x}_k(t) - \mathbf{x}_j(t)) \right\} - \frac{d}{dt}\mathbf{x}_j(t) \right], \quad (4)$$

where bold symbols are two-dimensional vectors.  $\mathbf{x}_j = (x_j, y_j)$  and  $\mathbf{x}_k = (x_k, y_k)$  are the positions of  $j$ th and  $k$ th particles, respectively.  $\mathbf{V}_0$  is a constant vector which expresses ‘‘desired velocity.’’ A particle moves with the desired velocity, if it is alone.  $\mathbf{F}$  expresses the interaction between particles and we choose the following form:

$$\mathbf{F}(\mathbf{x}_k - \mathbf{x}_j) = f(r_{kj})(1 + \cos \varphi)\mathbf{n}_{kj}, \quad (5)$$

$$f(r_{kj}) = \alpha[\tanh \beta(r_{kj} - b) + c], \quad (6)$$

where  $r_{kj} = |\mathbf{x}_k - \mathbf{x}_j|$ ,  $\cos \varphi = (x_k - x_j)/r_{kj}$  and  $\mathbf{n}_{kj} = (\mathbf{x}_k - \mathbf{x}_j)/r_{kj}$ . The strength of the interaction is determined by the distance



FIG. 1. A snapshot of the homogeneous flow. A triangular structure is observed in a numerical simulation with periodic boundary condition. All particles represented by black disks are moving rightward.

$r_{kj}$  between  $j$ th and  $k$ th particles and the angle  $\varphi$  between  $\mathbf{x}_k - \mathbf{x}_j$  and  $\mathbf{V}_0$ . Due to the term  $(1 + \cos \varphi)$ , a particle is more sensitive to particles in front than those behind. Equation (6) is nothing but the OV function for the one-dimensional model. We assume this form to understand both one- and two-dimensional phenomena in a unified way.

For convenience, we set  $\mathbf{V}_0 = (V_0, 0)$ , which means that particles are supposed to move in the positive direction of the  $x$  axis. We also set  $c \approx -1$ , that is,  $f < 0$ , which means that the interaction is repulsive [31,32]. This is a natural assumption for the interaction between pedestrians, but it is not essential in the analysis of the stability. The parameter  $\alpha$  is set to 1/4 for simplicity.

## III. LINEAR ANALYSIS

### A. Stability condition

In the same way as Ref. [19], we investigate the linear stability of homogeneous flow. To simplify the calculation, we remove the sensitivity  $a$  from the equation by the replacement  $t \rightarrow t/a$ ,  $V_0 \rightarrow aV_0$  and  $F \rightarrow aF$ . Equation (4) becomes

$$\frac{d^2}{dt^2}\mathbf{x}_j(t) = \mathbf{V}_0 + \sum_k \mathbf{F}(\mathbf{x}_k(t) - \mathbf{x}_j(t)) - \frac{d}{dt}\mathbf{x}_j(t). \quad (7)$$

By numerical simulations, we find that a flow shown in Fig. 1 is realized at a large distance (low density) [24]. We study the linear stability of this flow in this subsection. This homogeneous flow is expressed by the solution  $\mathbf{x}_j = \mathbf{X}_j + \mathbf{v}t$ . Here  $\mathbf{X}_j = (X_j, Y_j)$  is a constant vector which represents a site on a triangular lattice, and  $\mathbf{v} = (v_x, v_y)$  represents a constant velocity at which all particles move. The distances between any nearest-neighbor pairs are the same, and we use the distance as a parameter instead of the density.

We consider a small perturbation as follows:

$$x_j \rightarrow X_j + v_x t + x_j,$$

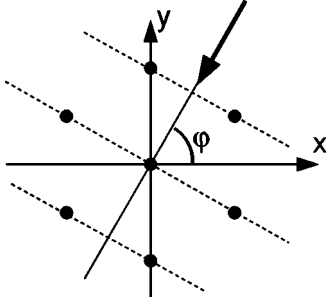
$$y_j \rightarrow Y_j + v_y t + y_j,$$

$$v_x = V_0 + \sum_k F_x(X_k - X_j, Y_k - Y_j),$$

$$v_y = \sum_k F_y(X_k - X_j, Y_k - Y_j), \quad (8)$$

where  $\mathbf{F} = (F_x, F_y)$ . The new  $x_j$  and  $y_j$  represent  $x$  and  $y$  components of the small deviation from the position  $(X_j, Y_j)$ .

From Eqs. (7) and (8), we can write the linearized equations


 FIG. 2. A wave propagating in the  $\varphi(=\pi/3)$  direction.

$$\frac{d^2}{dt^2}x_j = \sum_k [A_{kj}(x_k - x_j) + B_{kj}(y_k - y_j)] - \frac{d}{dt}x_j, \quad (9)$$

$$\frac{d^2}{dt^2}y_j = \sum_k [C_{kj}(x_k - x_j) + D_{kj}(y_k - y_j)] - \frac{d}{dt}y_j, \quad (10)$$

where parameters  $A_{kj}, B_{kj}, C_{kj}, D_{kj}$  are defined by

$$\begin{aligned} A_{kj} &= \partial_x F_x(x, y)|_{x=X_k-X_j, y=Y_k-Y_j}, \\ B_{kj} &= \partial_y F_x(x, y)|_{x=X_k-X_j, y=Y_k-Y_j}, \\ C_{kj} &= \partial_x F_y(x, y)|_{x=X_k-X_j, y=Y_k-Y_j}, \\ D_{kj} &= \partial_y F_y(x, y)|_{x=X_k-X_j, y=Y_k-Y_j}. \end{aligned} \quad (11)$$

Suppose that the small wave propagates at the angle  $\varphi$  with the  $x$  axis (see Fig. 2). Then the wave vector is  $\mathbf{k} = (k_x, k_y) = (k_x, pk_x)$  where  $p \equiv \tan \varphi$ . The two-dimensional wave is classified into two types of modes: longitudinal modes and transverse modes.

The longitudinal modes in the  $\varphi$  direction are written by

$$x_j = \exp[i\omega t + i\mathbf{k} \cdot \mathbf{x}] = \exp[i\omega t + i\theta(X_j + pY_j)], \quad (12)$$

$$y_j = px_j, \quad (13)$$

where  $\theta \equiv k_x$ . The linearized equations (9) and (10) are rewritten as

$$\frac{d^2}{dt^2}x_j = \sum_k (A_{kj} + pB_{kj})(x_k - x_j) - \frac{d}{dt}x_j, \quad (14)$$

$$0 = \sum_k \left( A_{kj} + pB_{kj} - \frac{1}{p}C_{kj} - D_{kj} \right) (x_k - x_j), \quad (15)$$

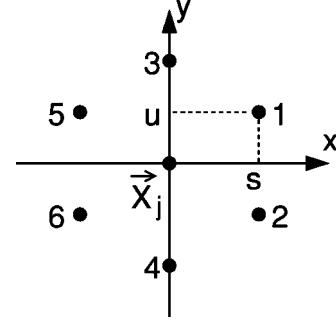
where the second equation is obtained by subtracting Eq. (10) from Eq. (9).

As for the transverse modes, we obtain the equations

$$x_j = \exp[i\omega t + i\mathbf{k} \cdot \mathbf{x}] \equiv \exp[i\omega t + i\theta(X_j + pY_j)], \quad (16)$$

$$y_j = -\frac{1}{p}x_j. \quad (17)$$

We note that  $\theta \equiv k_y$  in this case. The linearized equations are


 FIG. 3. Indices of six particles are shown. The positions of the particle 1, 2, 3, 4, 5, 6 are  $(s, u), (s, -u), (0, 2u), (0, -2u), (-s, u), (-s, -u)$ , respectively.

$$\frac{d^2}{dt^2}x_j = \sum_k \left( A_{kj} - \frac{1}{p}B_{kj} \right) (x_k - x_j) - \frac{d}{dt}x_j, \quad (18)$$

$$0 = \sum_k \left( A_{kj} - \frac{1}{p}B_{kj} + pC_{kj} - D_{kj} \right) (x_k - x_j). \quad (19)$$

Two special cases  $\varphi=0(p=0)$  and  $\varphi=\pi/2(p=\infty)$  should be investigated separately from the general case. That is, the analysis is carried out in three cases: (i) modes along the  $x$  axis ( $\varphi=0$ ), (ii) modes along the  $y$  axis ( $\varphi=\pi/2$ ), and (iii) other modes ( $0 < \varphi < \pi/2$ ).

In the homogeneous flow, the interaction with the nearest neighbors is dominant and we can neglect the interaction with further particles. Then the summation for  $k$  is taken over six particles around  $j$ th one. For convenience, we omit the index  $j$  and assign the number shown in Fig. 3 to the index  $k$ . For example, the position of particle 1 is  $(s, u) = (\sqrt{3}r/2, r/2)$  where  $r$  is the distance between two nearest-neighbor particles. The parameters in Eq. (11) are expressed as  $A_1, A_2, \dots, A_6, B_1, B_2, \dots, B_6$  [e.g.,  $A_1 = \partial_x F_x(x, y)|_{x=s, y=u}$ ]. The exact forms of these parameters are shown in Appendix A.

The stability condition should be investigated in three cases of directions of propagation for two polarizations. We solve Eq. (14) under the constraint (15) for the longitudinal modes and Eq. (18) under the constraint (19) for the transverse modes, and find the condition that  $\omega$  does not have negative imaginary part. The results are shown as follows, and the details are explained in Appendixes B–D.

The constraints (15) and (19) are automatically satisfied for the modes along the  $x$  axis, and we can easily find the stability conditions. The condition for the longitudinal mode along the  $x$  axis is

$$a > 2[1 + \cos(\theta s)] \frac{(A_1 - A_5)^2}{A_1 + A_5}, \quad (20)$$

and the condition for the transverse mode along the  $x$  axis is

$$a > 2[1 + \cos(\theta s)] \frac{(D_1 - D_5)^2}{D_1 + D_5}. \quad (21)$$

We note that Eqs. (20) and (21) are similar equations to the extended OV model for one-dimensional system [28–30].

The right-hand sides of Eqs. (20) and (21) take the maximum values at  $\theta=0$ , that is, the instability arises first from the longest wavelength mode for both cases. After substituting exact forms of  $A_1, A_5, D_1$  and  $D_5$ , we set  $\theta=0$ . Then we obtain the stability conditions for the homogeneous flow. The longitudinal modes are stable for

$$a > \frac{3[3f' + 2(f/r)]^2}{2[3f' + (f/r)]}, \quad (22)$$

and the transverse modes are stable for

$$a > \frac{3[f' + 2(f/r)]^2}{2[f' + 3(f/r)]}, \quad (23)$$

where  $r$  is the distance among particles, and  $f$  is the function (6) and  $f'$  is its derivative.

For off- $x$ -axis modes, there exist three remarkable points. First, the constraint (15) or (19) is satisfied only in the directions  $\varphi=n\pi/6$  ( $n=1, 2, 3, 4, 5, 7, 8, 9, 10, 11$ ), that is, no mode solutions exist in other directions. It is sufficient to analyze the stability in the three directions  $\varphi=\pi/6, \pi/3$  and  $\pi/2$ . Second, only the shortest wavelength mode is allowed in each direction and for each polarization (see Appendixes C and D). Third, the stability condition is decided only by the distance  $r$  independent of sensitivity  $a$ .

Consider the case of  $\varphi=\pi/2$  ( $y$  axis) as an example. Particles exist at intervals of the length  $u$  in the direction of the  $y$  axis. Therefore  $\theta=\pi/u$  is the largest wave number of the wave which propagates along the  $y$  axis. Each mode along the  $y$  axis is restricted to the mode with this wave number. Similar results are obtained in the directions  $\varphi=\pi/6, \pi/3$ . By solving Eq. (14) or (18) with the above results, we find the stability condition for each mode. For the longitudinal mode in the direction  $\varphi=\pi/2$  ( $y$  axis), the condition results in

$$D_1 + D_5 = \frac{1}{2}f' + \frac{3}{2}\left(\frac{f}{r}\right) > 0. \quad (24)$$

The stability condition for this mode does not depend on sensitivity  $a$  and depends only on the distance  $r$ . The similar conditions are obtained for modes in the direction  $\varphi=\pi/6, \pi/3$  (see Appendixes C and D). We note that this type of the stability condition appears in off- $x$ -axis directions.

### B. Phase structure

We can draw the phase diagram from the results in the previous subsection. As a typical case, we choose the parameters as  $\alpha=1/4, \beta=2.5, b=1.0, c=-1.0$  of the OV function (6). In Fig. 4, solid and dashed curves represent two critical curves defined by Eqs. (22) and (23). The longitudinal and transverse modes along the  $x$  axis become unstable in the region below the solid and dashed curve, respectively. Three critical lines  $r=1.05, r=0.94$ , and  $r=0.59$  correspond to the stability condition in the off- $x$  directions. Each mode in the off- $x$  direction is unstable in the left region of corresponding dotted line. All the stability conditions are summarized in Table I. We note that two critical values of distance  $r=0.59$  and  $r=1.05$  are common for various modes. These values also appear as the singularity of stability condition for the

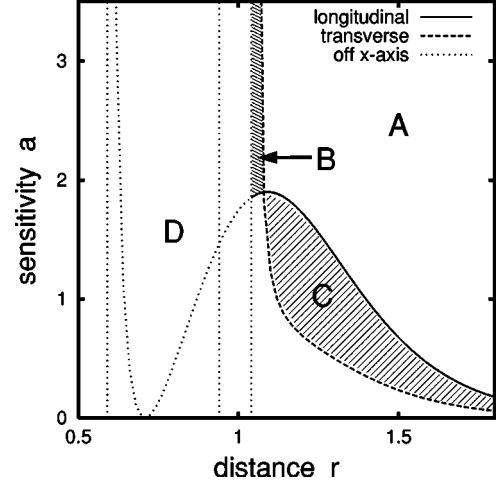


FIG. 4. The phase diagram obtained by the linear analysis. Solid and dashed curves represent the critical curves given by Eqs. (22) and (23), respectively. Dotted lines represent the critical lines  $r=1.05, r=0.94$ , and  $r=0.59$ . There are four phases that can be characterized by the type of unstable modes: longitudinal mode, transverse mode, and their mixture.

modes along the  $x$  axis: Equation (22) is singular at  $r=0.59$  and Eq. (23) is singular at  $r=1.05$ . The reason why the critical values for various modes coincide is not clear.

To summarize these results, the homogeneous flow is stable in the region A. In the region B, only the transverse modes along the  $x$  axis are unstable. In the region C, only the longitudinal modes along the  $x$  axis are unstable. The region C corresponds to the unstable region of the homogeneous flow in the one-dimensional system. However in the region D, several modes become unstable simultaneously and it is unpredictable within the linear analysis how the flow breaks. Therefore it is not clear whether dotted curves or lines in the region D are boundaries of phases or not. In the following section, we investigate the property of the flow in each phase by numerical simulations.

## IV. NUMERICAL SIMULATIONS

In this section, we show a typical behavior in each phase by numerical simulations. We adopt the periodic boundary condition in both directions of  $x$  and  $y$  axis for simplicity. The parameters are chosen the same values as those we have drawn the phase diagram by the linear analysis in Sec. III. In each phase, we choose appropriate values of sensitivity and

TABLE I. Stability conditions for all modes. Numerical values are calculated for the parameters  $\alpha=1/4, \beta=2.5, b=1.0$ , and  $c=-1.0$ .

$\varphi$	Longitudinal mode	Transverse mode
0 ( $x$ axis)	Eq. (22)	Eq. (23)
$\pi/6$	$r > 1.05$	$r > 0.59$
$\pi/3$	$r > 0.59$	$r > 1.05$
$\pi/2$ ( $y$ axis)	$r > 1.05$	$r > 0.94$

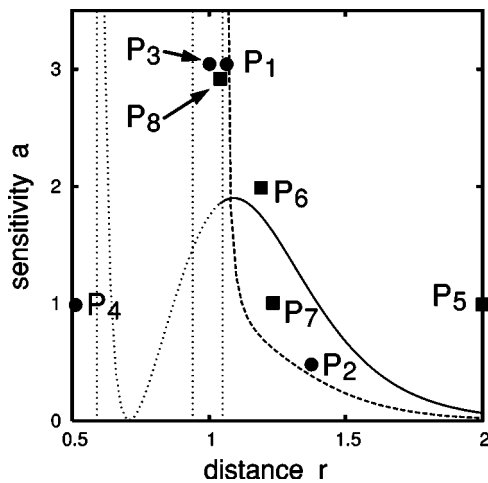


FIG. 5. Black disks  $P_1$ – $P_4$  and black squares  $P_5$ – $P_8$  represent parameters used in simulations for unidirectional flow and for counter flow, respectively.

the distance among particles. They are shown as points in the parameter space in Fig. 5. The point  $P_1$  is in the phase  $B$ , and  $P_2$  and  $P_7$  are in the phase  $C$ .  $P_5$  and  $P_6$  are in the phase  $A$ , and  $P_3$ ,  $P_4$  and  $P_8$  are in the phase  $D$ .

**A. Unidirectional flow**

First we carry out simulations for unidirectional flow, which corresponds to the situation investigated in the previous section. Figure 6 shows snapshots in the case of distance  $r=1.06$  and sensitivity  $a=3.0$ . This case corresponds to the point  $P_1$  in the phase  $B$  in Fig. 5. The simulation starts from the homogeneous flow [Fig. 6(a)], and after sufficient large time we observe the transverse wave [Fig. 6(b)].

Figure 7 shows snapshots for  $r=1.3$  and  $a=0.5$ , which correspond to the point  $P_2$  in the phase  $C$ . The simulation starts from the initial state shown in Fig. 6(a). Figure 7(a) shows the early stage where the longitudinal wave is ampli-

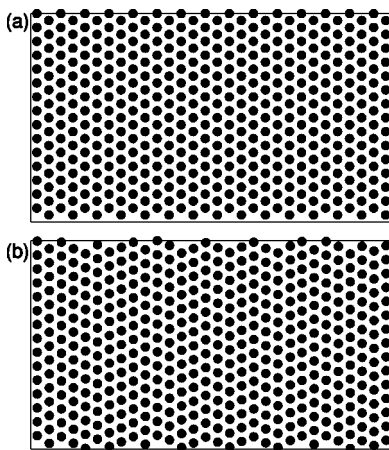


FIG. 6. A typical pattern of the flow at the point  $P_1$  in the phase  $B$ . Sensitivity  $a$  is set to 3.0, and the distance among particles  $r$  is 1.06. The initial state is the homogeneous flow (a) and the transverse wave is observed after relaxation (b).

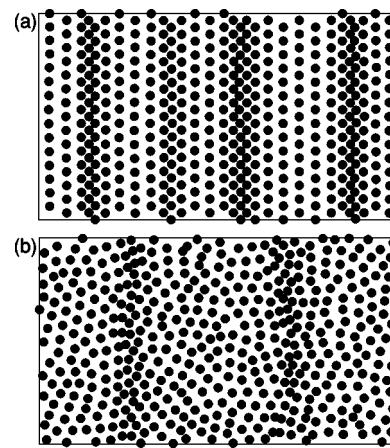


FIG. 7. A typical pattern of the flow at the early stage (a) and the flow after relaxation (b) at the point  $P_2$  ( $a=0.5, r=1.3$ ) in the phase  $C$ .

fied. The state after relaxation is shown in Fig. 7(b), where we can see clear density wave.

Figures 8 and 9 are snapshots of the states after relaxation for  $r=1.0, a=3.0$  ( $P_3$  in Fig. 5) and  $r=0.5, a=1.0$  ( $P_4$  in Fig. 5), respectively. In these cases, simulations start from the same initial state shown in Fig. 6(a). The states in Figs. 7(b), 8, and 9 ( $P_2, P_3, P_4$ ) transit to each other continuously by the change of parameters  $r$  and  $a$ . It is difficult to find clear borders among them. In the result, we can clearly distinguish the behaviors in the phases  $A, B$  and  $C$ : the homogeneous flow in phase  $A$ , the transverse wave in phase  $B$  and the longitudinal wave in phase  $C$ . However, the border between phases  $C$  and  $D$  is not clear from the results of simulations.

**B. Counter flow**

Interesting phenomena in pedestrian flow are observed in counter flow. Here we suggest a mechanism for such phenomena based on our analysis.

Figure 10 is the result of simulations of counter flow at large  $r$  (low density). The figure shows two snapshots after sufficient relaxation time. White or black particles are moving leftward and rightward, respectively. We set that a half number of particles move in the opposite direction,  $\mathbf{V}_0 = (-V_0, 0)$ . In Fig. 10(a), we choose parameters as  $r=2.0$  and

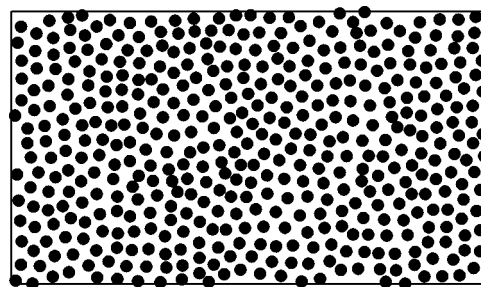


FIG. 8. A snapshot of the flow after relaxation. Parameters are  $a=3.0$  and  $r=1.0$  ( $P_3$  in Fig. 5). Particles move randomly but a triangular structure emerges partly.

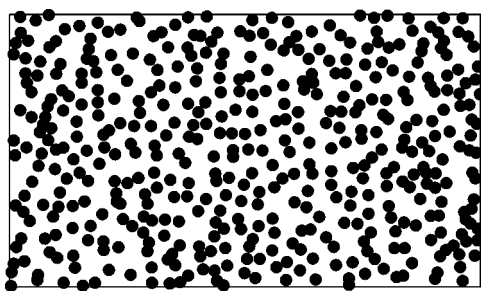


FIG. 9. A snapshot of the flow after relaxation. Parameters are  $a=1.0$  and  $r=0.5$  ( $P_4$  in Fig. 5). Particles move randomly and no structure is observed.

$a=1.0$  ( $P_5$  in Fig. 5), and in Fig. 10(b), we choose  $r=1.2$  and  $a=2.0$  ( $P_6$ ). Clear lanes are formed, where particles are moving in the opposite directions (lane separation). The formed lanes are stable, since the unidirectional homogeneous flow is stable at the points  $P_5$  and  $P_6$ . Each lane can be considered as unidirectional flow, and the stability condition is roughly the same as that obtained for unidirectional flow. In the case that the lane is a single line of particles, it is essentially a one-dimensional system, and the stability condition is the same as the original OV model.

When the distance among particles is a little smaller than the critical value obtained by the analysis of unidirectional flow, the temporal lane formation is observed but these lanes are unstable. The final states in such cases are shown in Fig. 11. These are blocking states. Particles cannot move smoothly, because their motion is prevented by other particles coming in the opposite direction. At shorter distance ( $r < 1$ ), no temporal lane formation is observed, and the blocking state emerges immediately. The blocking state in our model is not completely frozen [8], because we treat pedestrians as point particles for simplicity. Particles move windingly in the crowd and pass through a tiny space be-

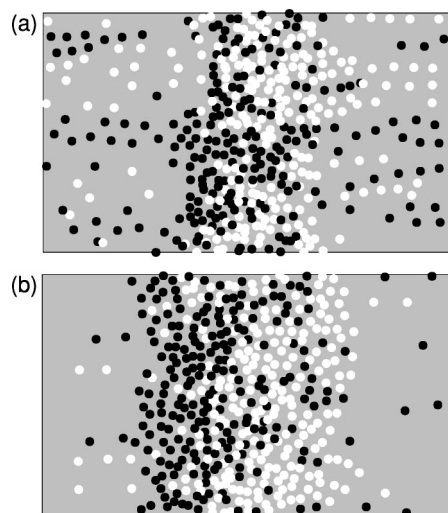


FIG. 11. Typical blocking states of counter flow at the points (a)  $P_7(a=1.0, r=1.24)$  and (b)  $P_8(a=3.0, r=1.04)$ . White or black disks are particles moving leftward and rightward, respectively. Boundary conditions are periodic in both  $x$  and  $y$  directions.

tween particles, and finally escape to the opposite side of the crowd.

The simulations in Fig. 11 are performed at the point  $P_7(a=1.0$  and  $r=1.24)$  in the region  $C$  in Fig. 4, and the point  $P_8(r=1.04$  and  $a=3.0)$  in the region  $D$ . From the results of simulations, we conclude that the lane formation occurs in the region  $A$  where the homogeneous flow is stable, and the blocking occurs in the region where the homogeneous flow is unstable. A rough sketch of the phase diagram for counter flow is as follows. There are two phases; in one phase the lane formation occurs, and in the other phase the blocking occurs. The boundary between above two phases exists near the boundary between the region  $A$  and  $B(C)$  in unidirectional flow (Fig. 4).

### V. SUMMARY AND DISCUSSION

In this paper, we investigated the linear stability of the homogeneous flow solution in the two-dimensional OV model [24–27]. We found two types of instability of mode solutions. One is the instability of modes propagating in the direction of the desired velocity ( $x$  axis). The stability conditions of these modes (transverse and longitudinal) depend on the sensitivity  $a$  and the distance  $r$  between nearest-neighbor particles. The other is the instability of modes which propagate in the off- $x$ -axis direction. Such modes exist only in the directions with the angle  $\varphi = n\pi/6$  ( $n=1, 2, 3, 4, 5, 7, 8, 9, 10, 11$ ). Moreover, only the shortest wavelength mode is allowed in each direction and for each polarization. The stability conditions for off- $x$ -axis modes depend only on the distance  $r$  and not on the sensitivity  $a$ . These properties are remarkable differences from those of the modes along the  $x$  axis.

From the results of the linear analysis, we can draw the phase diagram. There exist roughly four phases: phase  $A$  (the region  $A$  in Fig. 4) where the homogeneous flow is stable,

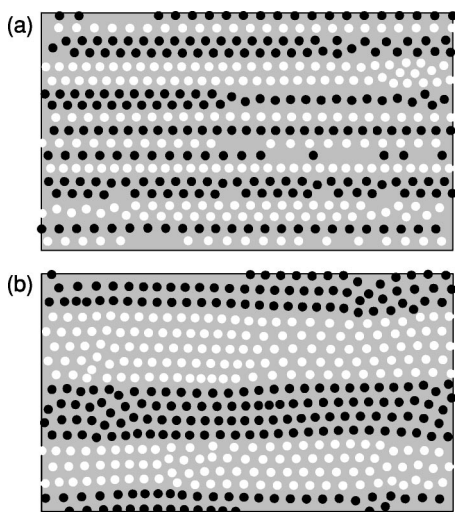


FIG. 10. Typical stationary patterns of counter flow at the points (a)  $P_5(a=1.0, r=2.0)$  and (b)  $P_6(a=2.0, r=1.2)$  in the region  $A$ . White or black disks represent particles moving leftward and rightward, respectively. Boundary conditions are periodic in both  $x$  and  $y$  directions.

phase *B* where the transverse modes along the *x* axis are unstable, phase *C* where the longitudinal modes along the *x* axis are unstable and phase *D* where several modes are unstable. The value of sensitivity decides which type of instability occurs. The instability of transverse mode (phases *B*) occurs in high sensitivity and high density. In contrast, the instability of longitudinal mode (phase *C*) occurs in low sensitivity and comparably low density. We carried out numerical simulation to investigate the behavior of flow in each phase. We can distinguish the behaviors in the phases *A*, *B* and *C*. However, the behaviors in the phases *C* and *D* seem to transit each other continuously.

We also perform numerical simulations of counter flow. The lane formation occurs at a large distance (low density) and the blocking occurs at a small distance (high density). The border between these two states exists near the critical curve of the stability condition for the unidirectional flow. The transition from the lane formed state to the blocking state can be explained as follows. When the lanes are formed, there is almost no interaction between particles moving in different lanes. Each lane can be considered as unidirectional flow and is stable at the density where the homogeneous flow is stable (phase *A* in Fig. 4). If the density is a little higher (phase *B* and phase *C*), lanes are formed temporarily. Each lane cannot be maintained due to the unstable modes in the *x* direction and the blocking phenomenon occurs finally. At much higher density, several modes in the off-*x* direction are unstable simultaneously, and the blocking state emerges immediately. The results of simulations in counter flow can be understood by use of the results of linear analysis for unidirectional flow. Therefore we conclude that the two-dimensional OV model can present a unified understanding of these phenomena in pedestrian flow.

Beyond the analysis for the pedestrian flow, the model can be applied to granular flow in liquid through a vertical pipe. It is well known that the granular flow shows a similar phenomena to traffic congestion. The emergence of jam clusters can be understood in the framework of the OV model, because the analysis does not depend on the detail of the OV function. A congestion phenomenon is a common feature in the system similar to traffic flow. It is not essential that the difference between the interaction among granules and the interaction among pedestrians.

#### ACKNOWLEDGMENT

This work is partly supported by a Grant-in-Aid for Scientific Research (C) (No.15560051) of the Japanese Ministry of Education, Science, Sports and Culture.

#### APPENDIX A: EXACT FORMS OF *A*, *B*, *C*, *D*

The exact forms of parameters defined by Eq. (11) are as follows:

$$A_1 = A_2 = f' \left( \frac{3}{4} + \frac{3\sqrt{3}}{8} \right) + \frac{f}{r} \left( \frac{1}{4} + \frac{\sqrt{3}}{4} \right), \quad (\text{A1})$$

$$A_3 = A_4 = \frac{f}{r}, \quad (\text{A2})$$

$$A_5 = A_6 = f' \left( \frac{3}{4} - \frac{3\sqrt{3}}{8} \right) + \frac{f}{r} \left( \frac{1}{4} - \frac{\sqrt{3}}{4} \right), \quad (\text{A3})$$

$$B_1 = -B_2 = f' \left( \frac{3}{8} + \frac{\sqrt{3}}{4} \right) + \frac{f}{r} \left( -\frac{3}{4} - \frac{\sqrt{3}}{4} \right), \quad (\text{A4})$$

$$B_3 = -B_4 = 0, \quad (\text{A5})$$

$$B_5 = -B_6 = f' \left( \frac{3}{8} - \frac{\sqrt{3}}{4} \right) + \frac{f}{r} \left( -\frac{3}{4} + \frac{\sqrt{3}}{4} \right), \quad (\text{A6})$$

$$C_1 = -C_2 = f' \left( \frac{3}{8} + \frac{\sqrt{3}}{4} \right) + \frac{f}{r} \left( -\frac{1}{4} - \frac{\sqrt{3}}{4} \right), \quad (\text{A7})$$

$$C_3 = -C_4 = \frac{f}{r}, \quad (\text{A8})$$

$$C_5 = -C_6 = f' \left( \frac{3}{8} - \frac{\sqrt{3}}{4} \right) + \frac{f}{r} \left( -\frac{1}{4} + \frac{\sqrt{3}}{4} \right), \quad (\text{A9})$$

$$D_1 = D_2 = f' \left( \frac{1}{4} + \frac{\sqrt{3}}{8} \right) + \frac{f}{r} \left( \frac{3}{4} + \frac{\sqrt{3}}{4} \right), \quad (\text{A10})$$

$$D_3 = D_4 = f', \quad (\text{A11})$$

$$D_5 = D_6 = f' \left( \frac{1}{4} - \frac{\sqrt{3}}{8} \right) + \frac{f}{r} \left( \frac{3}{4} - \frac{\sqrt{3}}{4} \right). \quad (\text{A12})$$

#### APPENDIX B: MODES ALONG *x* AXIS

##### 1. Longitudinal modes

In this case ( $p=0$ ), the equations corresponding to Eqs. (12)–(15) are

$$x_j = \exp[i\omega t + i\mathbf{k} \cdot \mathbf{x}] = \exp[i\omega t + i\theta X_j], \quad (\text{B1})$$

$$y_j = 0, \quad (\text{B2})$$

and

$$\frac{d^2}{dt^2} x_j = \sum_k A_{kj} (x_k - x_j) - \frac{d}{dt} x_j, \quad (\text{B3})$$

$$0 = \sum_k C_{kj} (x_k - x_j). \quad (\text{B4})$$

We can easily find that Eq. (B4) is automatically satisfied as follows:

$$\begin{aligned} \sum_k C_{kj} (x_k - x_j) &= \sum_k C_{kj} [e^{i\theta X_k} - e^{i\theta X_j}] e^{i\omega t} \\ &\propto (C_1 + C_2)(e^{i\theta s} - 1) + (C_5 + C_6)(e^{-i\theta s} - 1) \\ &= 0. \end{aligned} \quad (\text{B5})$$

Equation (B3) becomes

$$-\omega^2 = 2A_1(e^{i\theta s} - 1) + 2A_5(e^{-i\theta s} - 1) - i\omega. \quad (\text{B6})$$

This is the same equation as the extended OV model for one-dimensional system [28–30]. Therefore we can easily find the stability condition for the mode (B1):

$$a > 2[1 + \cos(\theta s)] \frac{(A_1 - A_5)^2}{A_1 + A_5}, \quad (\text{B7})$$

where the sensitivity  $a$  is restored by  $f \rightarrow f/a$ .

## 2. Transverse modes

The transverse modes along the  $x$  axis are expressed as

$$x_j = 0, \quad (\text{B8})$$

$$y_j = \exp[i\omega t + i\mathbf{k} \cdot \mathbf{x}] = \exp[i\omega t + i\theta X_j], \quad (\text{B9})$$

and Eqs. (9) and (10) become

$$0 = \sum_k B_{kj}(y_k - y_j), \quad (\text{B10})$$

$$\frac{d^2}{dt^2} y_j = \sum_k D_{kj}(y_k - y_j) - \frac{d}{dt} y_j. \quad (\text{B11})$$

We can easily verify that Eq. (B10) is satisfied in the same way as Eq. (B5). Equation (B11) also gives the similar equation to Eq. (B6), and therefore the stability condition for this mode is

$$a > 2[1 + \cos(\theta s)] \frac{(D_1 - D_5)^2}{D_1 + D_5}. \quad (\text{B12})$$

## APPENDIX C: MODES ALONG $y$ AXIS

### 1. Longitudinal modes

The longitudinal modes along the  $y$  axis ( $p=\infty$ ) are written as

$$x_j = 0, \quad (\text{C1})$$

$$y_j = \exp[i\omega t + i\mathbf{k} \cdot \mathbf{x}] = \exp[i\omega t + i\theta Y_j], \quad (\text{C2})$$

and Eqs. (9) and (10) become

$$0 = \sum_k B_{kj}(y_k - y_j), \quad (\text{C3})$$

$$\frac{d^2}{dt^2} y_j = \sum_k D_{kj}(y_k - y_j) - \frac{d}{dt} y_j. \quad (\text{C4})$$

Equation (C3) gives a nontrivial constraint

$$0 = (e^{i\theta u} - e^{-i\theta u})(B_1 + B_5). \quad (\text{C5})$$

In the present case, we can easily find  $B_1 + B_5 \neq 0$ , and the solution is

$$\theta = \frac{n\pi}{u}, \quad (\text{C6})$$

where  $n$  is an integer. Here  $n \neq 1$  is meaningless because  $u$  is the minimal length of  $|Y_k - Y_j|$ . Therefore  $\theta = \pi/u$  is the only mode which propagates in the  $y$  direction.

Inserting Eq. (C2) into Eq. (C4), we find

$$-\omega^2 = -4(D_1 + D_5) - i\omega, \quad (\text{C7})$$

where we used  $\theta u = \pi$ . The stability condition for this mode is given by

$$D_1 + D_5 = \frac{1}{2}f' + \frac{3}{2}\left(\frac{f}{r}\right) > 0. \quad (\text{C8})$$

As an example, we set parameters as  $\alpha=1/4, \beta=2.5, b=1.0, c=-1.0$ . Then Eq. (C8) is satisfied for  $r > 1.05$ .

### 2. Transverse modes

The transverse modes are

$$x_j = \exp[i\omega t + i\mathbf{k} \cdot \mathbf{x}] = \exp[i\omega t + i\theta Y_j], \quad (\text{C9})$$

$$y_j = 0, \quad (\text{C10})$$

and the equations are

$$\frac{d^2}{dt^2} x_j = \sum_k A_{kj}(x_k - x_j) - \frac{d}{dt} x_j, \quad (\text{C11})$$

$$0 = \sum_k C_{kj}(x_k - x_j). \quad (\text{C12})$$

The constraint (C12) becomes

$$0 = (e^{i\theta u} - e^{-i\theta u})\{C_1 + C_5 + C_3(e^{i\theta u} + e^{-i\theta u})\}, \quad (\text{C13})$$

and this is satisfied in the following two cases.

(1)  $(e^{i\theta u} - e^{-i\theta u}) = 0$ . In the same way as the previous subsection, we find  $\theta u = \pi$  and the stability condition

$$A_1 + A_5 = \frac{3}{2}f' + \frac{1}{2}\left(\frac{f}{r}\right) > 0. \quad (\text{C14})$$

This condition is satisfied if  $r > 0.59$  for the same parameters as Appendix C 1.

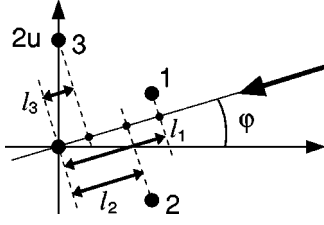
(2)  $C_1 + C_5 + C_3(e^{i\theta u} + e^{-i\theta u}) = 0$ . Because  $C_3 \neq 0$ , the solution is

$$\cos(\theta u) = -\frac{C_1 + C_5}{2C_3}. \quad (\text{C15})$$

Therefore Eq. (C11) becomes

$$-\omega^2 = \left[ -2(A_1 + 2A_3 + A_5) - \frac{(A_1 + A_5)(C_1 + C_5)}{C_3} + A_3 \frac{(C_1 + C_5)^2}{C_3^2} \right] - i\omega. \quad (\text{C16})$$

From the first term of the right-hand side of Eq. (C16), we find the stability condition


 FIG. 12. Parameters  $l_1, l_2$ , and  $l_3$  are graphically shown.

$$-\frac{r}{f} \left[ f' + 2\frac{f}{r} \right] \left[ f' + 4\frac{f}{r} \right] > 0. \quad (\text{C17})$$

In this case, the necessary condition for the stability is not only Eq. (C17) but also the condition that Eq. (C15) has a solution. We can find the range of  $r$  numerically and the result is  $r > 0.94$ .

## APPENDIX D: MODE IN GENERAL DIRECTION

### 1. Longitudinal modes

For the stability of longitudinal modes in the direction ( $0 < \varphi < \pi/2$ ), we simplify the equations first. By use of the mode function (12), the constraint (15) is rewritten as

$$\begin{aligned} 0 = & e^{i\theta(s+pu)} \left( A_1 - D_1 + pB_1 - \frac{1}{p}C_1 \right) + e^{i\theta(s-pu)} \left( A_1 - D_1 - pB_1 \right. \\ & \left. + \frac{1}{p}C_1 \right) + e^{2i\theta pu} \left( A_3 - D_3 - \frac{1}{p}C_3 \right) + e^{-2i\theta pu} \left( A_3 - D_3 \right. \\ & \left. + \frac{1}{p}C_3 \right) + e^{-i\theta(s-pu)} \left( A_5 - D_5 + pB_5 - \frac{1}{p}C_5 \right) \\ & \left. + e^{-i\theta(s+pu)} \left( A_5 - D_5 - pB_5 + \frac{1}{p}C_5 \right). \end{aligned} \quad (\text{D1})$$

Because  $s = \sqrt{3}r/2$  and  $u = r/2$ , the equation can be simplified by the replacement  $p = \sqrt{3}/q$ , where  $q$  is a real number. Note that  $q=1$  and  $q=3$  correspond to  $\varphi = \pi/3$  and  $\varphi = \pi/6$ , respectively. The arguments of exponential functions in Eq. (D1) become

$$2\theta pu = \frac{\sqrt{3}}{q} r \theta \equiv 2\phi, \quad s \pm pu = \left( \frac{\sqrt{3}}{2} \pm \frac{\sqrt{3}}{2q} \right) r = (q \pm 1)\phi. \quad (\text{D2})$$

The meaning of the parametrization is shown in Fig. 12. Note  $2\phi = 2\theta pu = |k|l_3$ , where  $l_3 = 2u \sin \varphi$  is the length of projection of  $(0, 2u)$  to the direction of vector  $\mathbf{k}$  and  $\theta = k_x = |k| \cos \varphi$ . Similarly,  $(q+1)\phi = |k|l_1$  and  $(q-1)\phi = |k|l_2$ , where  $l_1$  and  $l_2$  are the lengths of projection of  $(s, u)$  and  $(s, -u)$ , respectively. Figure 12 shows the situation for  $q > 3$ , and in such a case  $l_3$  is the minimum length among them. Therefore  $2\phi = \pi$  corresponds to the largest wave number of modes which propagate in the  $\varphi$  direction shown in Fig. 12.

In the notation (D2), Eq. (D1) is rewritten as

$$\begin{aligned} 0 = & e^{i(q+1)\phi} \left( A_1 - D_1 + pB_1 - \frac{1}{p}C_1 \right) + e^{-i(q+1)\phi} \left( A_5 - D_5 - pB_5 \right. \\ & \left. + \frac{1}{p}C_5 \right) + e^{i(q-1)\phi} \left( A_1 - D_1 - pB_1 + \frac{1}{p}C_1 \right) \\ & + e^{-i(q-1)\phi} \left( A_5 - D_5 + pB_5 - \frac{1}{p}C_5 \right) + e^{2i\phi} \left( A_3 - D_3 - \frac{1}{p}C_3 \right) \\ & \left. + e^{-2i\phi} \left( A_3 - D_3 + \frac{1}{p}C_3 \right). \end{aligned} \quad (\text{D3})$$

This constraint decides the value of  $\phi$ , that is,  $k$ , depending on  $r$  for given  $q \sim \varphi$ . Here we consider the modes whose wave number  $k$  is independent of distance  $r$ . The parameters  $A_1, \dots, D_6$  consist of two terms: one is proportional to  $f(r)/r$  and the other is proportional to  $f'(r)$  (see Appendix A). Therefore both coefficients of  $f(r)/r$  and  $f'(r)$  in the constraint (D3) must be zero [33]. As a result, we obtain two complex-valued conditions from Eq. (D3), which reduce to four real-valued conditions. Because two among four conditions are identical, three conditions remain as follows:

$$\begin{aligned} 0 = & (q-3)(q+1)\cos(q+1)\phi - (q+3)(q-1)\cos(q-1)\phi \\ & + 4q \cos 2\phi, \\ 0 = & (q-3)(q+3)\sin(q+1)\phi - (q+3)(q-3)\sin(q-1)\phi \\ & - 4q^2 \sin 2\phi, \\ 0 = & (q-3)(q+1)\sin(q+1)\phi - (q+3)(q-1)\sin(q-1)\phi. \end{aligned} \quad (\text{D4})$$

We found the solutions only for  $q=1$  or  $q=3$ . For general  $q$ , we have investigated the existence of solutions numerically, and could not find any other solutions.

Here we show the results.

(1)  $q=1$  ( $\varphi = \pi/3$ ). In this case, Eqs. (D4) become

$$\begin{aligned} 0 = & -4 \cos 2\phi + 4 \cos 2\phi, \\ 0 = & -8 \sin 2\phi - 4 \sin 2\phi, \\ 0 = & -4 \sin 2\phi, \end{aligned} \quad (\text{D5})$$

and are reduced to a single equation  $\sin 2\phi = 0$ . Only the mode  $2\phi = \pi$  exists and the stability condition of this mode is

$$3f' + \frac{f}{r} > 0. \quad (\text{D6})$$

This is the same condition as Eq. (C14) and the mode is stable for  $r > 0.59$ .

(2)  $q=3$  ( $\varphi = \pi/6$ ). Also in this case, only the mode  $2\phi = \pi$  exists. The stability condition is

$$f' + 3\frac{f}{r} > 0. \quad (\text{D7})$$

This is the same condition as Eq. (C8) and the mode is stable for  $r > 1.05$ .

## 2. Transverse modes

For the transverse modes in the direction ( $0 < \varphi < \pi/2$ ), the constraint (19) becomes

$$0 = e^{i(q+1)\phi} \left( A_1 - D_1 - \frac{1}{p} B_1 + p C_1 \right) + e^{-i(q+1)\phi} \left( A_5 - D_5 + \frac{1}{p} B_5 - p C_5 \right) + e^{i(q-1)\phi} \left( A_1 - D_1 + \frac{1}{p} B_1 - p C_1 \right) + e^{-i(q-1)\phi} \left( A_5 - D_5 - \frac{1}{p} B_5 + p C_5 \right) + e^{2i\phi} (A_3 - D_3 + p C_3) + e^{-2i\phi} (A_3 - D_3 + p C_3), \quad (\text{D8})$$

where we used  $p = \sqrt{3}/q$  and  $2\theta pu = 2\phi$ . In the same way as the previous subsection, we find three conditions

$$0 = (q-3)(q+1)\cos(q+1)\phi - (q+3)(q-1)\cos(q-1)\phi + 4q \cos 2\phi,$$

$$0 = (q-1)(q+1)\sin(q+1)\phi - (q+1)(q-1)\sin(q-1)\phi + 4 \sin 2\phi,$$

$$0 = (q-3)(q+1)\sin(q+1)\phi - (q+3)(q-1)\sin(q-1)\phi. \quad (\text{D9})$$

In Eqs. (D9), only the second equation is different from that in Eqs. (D4).

The solutions exist only for  $q=1$  and  $q=3$ . The results are as follows.

(1)  $q=1$  ( $\varphi = \pi/3$ ). Only the mode  $2\phi = \pi$  exists and the stability condition of this mode is

$$f' + 3\frac{f}{r} > 0. \quad (\text{D10})$$

This is the same condition as Eq. (C8) and the mode is stable for  $r > 1.05$ .

(2)  $q=3$  ( $\varphi = \pi/6$ ). Only the mode  $2\phi = \pi$  exists and the stability condition is

$$3f' + \frac{f}{r} > 0. \quad (\text{D11})$$

This is the same condition as Eq. (C14) and the mode is stable for  $r > 0.59$ .

- 
- [1] *Workshop on Traffic and Granular Flow*, edited by D. E. Wolf, M. Schreckenberg, and A. Bachem (World Scientific, Singapore, 1996).
- [2] *Workshop on Traffic and Granular Flow '97*, edited by M. Schreckenberg and D. E. Wolf (Springer-Verlag, Singapore, 1998).
- [3] *Traffic and Granular Flow '99*, edited by D. Helbing, H. J. Herrmann, M. Schreckenberg, and D. E. Wolf (Springer-Verlag, Berlin, 2000).
- [4] *Traffic and Granular Flow '01*, edited by M. Fukui, Y. Sugiyama, M. Schreckenberg, and D. E. Wolf (Springer-Verlag, Berlin, 2003).
- [5] D. Chowdhury, L. Santen, and A. Schadschneider, *Phys. Rep.* **329**, 199 (2000).
- [6] D. Helbing, *Rev. Mod. Phys.* **73**, 1067 (2001).
- [7] D. Helbing, in *Traffic and Granular Flow '97*, edited by M. Schreckenberg and D. E. Wolf (Springer-Verlag, Singapore, 1998), pp. 21–36.
- [8] D. Helbing, I. J. Frakas, and T. Vicsek, in *Traffic and Granular Flow '99* (Ref. [3]), pp. 245–250.
- [9] L. F. Henderson, *Transp. Res.* **8**, 509 (1974).
- [10] P. G. Gipps and B. Marksjö, *Math. Comput. Simul.* **27**, 95 (1985).
- [11] D. Helbing and P. Molnar, *Phys. Rev. E* **51**, 4282 (1995).
- [12] R. L. Hughes, *Math. Comput. Simul.* **53**, 367 (2000).
- [13] C. Burstedde, K. Klauk, A. Schadschneider, and J. Zittartz, *Physica A* **295**, 507 (2001).
- [14] A. Kirchner and A. Schadschneider, *Physica A* **312**, 260 (2002).
- [15] A. Kirchner, H. Klüpfel, K. Nishinari, A. Schadschneider, and M. Schreckenberg, *Physica A* **324**, 689 (2003).
- [16] A. Kirchner, K. Nishinari, and A. Schadschneider, *Phys. Rev. E* **67**, 056122 (2003).
- [17] *Pedestrian and Evacuation Dynamics*, edited by M. Schreckenberg and S. D. Sharma (Springer-Verlag, Berlin, 2002).
- [18] *Pedestrian and Evacuation Dynamics 2003*, edited by E. R. Galea (CMS Press, Greenwich, 2003).
- [19] M. Bando, K. Hasebe, A. Nakayama, A. Shibata, and Y. Sugiyama, *Phys. Rev. E* **51**, 1035 (1995).
- [20] M. Bando, K. Hasebe, A. Nakayama, A. Shibata, and Y. Sugiyama, *Jpn. J. Ind. Appl. Math.* **11**, 203 (1994).
- [21] M. Bando, K. Hasebe, K. Nakanishi, A. Nakayama, A. Shibata, and Y. Sugiyama, *J. Phys. I* **5**, 1389 (1995).
- [22] S. Horikawa, A. Nakahara, T. Nakayama, and M. Matsushita, *J. Phys. Soc. Jpn.* **64**, 1870 (1995).
- [23] O. Moriyama, N. Kuroiwa, M. Matsushita, and H. Hayakawa, *Phys. Rev. Lett.* **80**, 2833 (1998).
- [24] Y. Sugiyama, A. Nakayama, and K. Hasebe, in *Pedestrian and Evacuation Dynamics* (Ref. [17]), pp. 155–160.
- [25] Y. Sugiyama, A. Nakayama, and K. Hasebe, in *Traffic and Granular Flow '01* (Ref. [4]), pp. 537–542.
- [26] A. Nakayama, K. Hasebe, and Y. Sugiyama, in *Traffic and Granular Flow '01* (Ref. [4]), pp. 127–140.
- [27] A. Nakayama and Y. Sugiyama, in *Pedestrian and Evacuation Dynamics 2003* (Ref. [18]), p. 409.
- [28] K. Hasebe, A. Nakayama, and Y. Sugiyama, *Phys. Rev. E* **65**, 016112 (2001).
- [29] K. Hasebe, A. Nakayama, and Y. Sugiyama, in *Traffic and Granular Flow '01* (Ref. [4]), pp. 221–226.
- [30] K. Hasebe, A. Nakayama, and Y. Sugiyama, *Phys. Rev. E* **68**, 026102 (2003).

- [31] A. Nakayama and Y. Sugiyama, in *Modeling of Complex Systems: Seventh Granada Lectures*, edited by P. L. Garrido and J. Marro (AIP, Melville, NY, 2003), pp. 107–110.
- [32] In the model with  $c > -1$ , both repulsive and attractive interactions exist [31]. Such a model is suitable for collective

motion of biological system.

- [33] We can find another condition which is satisfied only for a specific  $r$ . There may be instability due to this mode, but it could not be observed in numerical simulations.